Applied Thermal Engineering 234 (2023) 121195

Contents lists available at ScienceDirect

Applied Thermal Engineering

journal homepage: www.elsevier.com/locate/ate

Research Paper

Evaluation of GDI spray structures under flash boiling and strong collapse conditions with diverse fuels

Raul Payri [a,*], P. Marti-Aldaravi [a], Victor Mendoza Alvarez [a], Abian Bautista [b]

[a] CMT - Motores Térmicos, Universitat Politècnica de València, Edificio 6D, 46022, Valencia, Spain
[b] MAHLE Electronics S.L.U., 46980, Paterna, Valencia, Spain

ARTICLE INFO

Keywords:
GDI
Gasoline
Engine
Flash-boiling
Spray collapse
Optical techniques

ABSTRACT

GDI (Gasoline Direct Injection) sprays are a matter of continuous research due to their potential for higher thermal efficiency and power output. Injections in GDI engines tend to happen at relatively high temperatures, which, combined with volatile fuels, are a perfect environment for flashing sprays, which are present in recently developed GDI engine passenger cars. Phenomena like flash boiling and especially spray collapse are still being investigated due to their complexity and impact on the engine performance. In the present research, the impact of different levels of flash boiling in the sprays is analyzed. Four surrogate mono-component fuels were tested with different volatile properties. Two optical techniques were carried out simultaneously: light extinction images (DBI) and frontal MIE scattering. The spray width was used to represent the radial expansion and study its relation with the spray collapse due to flash boiling. The degree of collapse was quantified by means of the instantaneous spray width variation for which three levels of collapse were identified. A novel MIE frontal approach was employed to study the spray surface evolution and the collapsing time by monitoring the nozzle tip clouding (opaquing) by the fuel. Results showed an increment of the width with the ratio of saturation to ambient pressure (R_p), as well as a strong correlation between the spray surface and the R_p at each fuel temperature when the spray is stabilized. Based on the MIE technique, three collapse instants were identified throughout the injection time depending on the R_p.

1. Introduction

Thanks to the increase of GDI engines in the market, some of the most distinct phenomena in this type of engine are regaining space in the research interest. One of the latest concerns gaining more importance in the field is the flash boiling phenomenon. The future development targets for new GDI engines include reducing fuel consumption, improving engine performance with minimum compromise on fuel economy, and meeting the existing and upcoming emission regulations [1,2]. Projections of the car market for the next decades indicate that low carbon fossil fuel passenger cars will still have an essential share of the car market in the world [3]. Even some countries will not be capable of keeping up with Europe and USA in the electrification area and will still be using and demanding gasoline cars by 2050 [4].

In GDI, the fuel is directly injected into the cylinder; thus, the injection takes place at relatively high temperatures, which, together with volatile fuels and low ambient pressure, promote phenomena such as flash boiling, as well as sudden changes in the spray structure [1], being beneficial for some cases, but also, bringing difficulties in predicting the spray characteristics for all operation conditions, and consequently, the charge formation repeatability.

As mentioned by Krämer et al. [5], something to consider is that during some of the recent European Driving Cycle, up to 95% of injections are superheated which favors the flash boiling and spray collapse phenomenon [6]. The flash boiling is a sudden phase change phenomenon that influences the spray formation process. Under the same operating injection pressure, flash boiling sprays are distinguished by lower droplet mean diameter, greater homogeneity, and shorter penetration in an isolated spray plume. [7]. This phenomenon involves several physical processes such as nucleation, bubble growth, two-phase flow, and atomization [8]. Flash boiling can occur in different situations during the regular operation of a car engine.

The flash boiling can be represented by the superheated degree of the fuel at the operating condition. It is expressed in the literature by the temperature difference (ΔT) between liquid and saturation temperatures, or the ratio of saturation pressure to ambient pressure (Eq. (1)), also named R_p (used in this article). The R_p has been used to classify the level of flash boiling, being that for $R_p < 1$ it is

* Corresponding author.
E-mail address: rpayri@mot.upv.es (R. Payri).

https://doi.org/10.1016/j.applthermaleng.2023.121195
Received 22 February 2023; Received in revised form 16 May 2023; Accepted 17 July 2023
Available online 20 July 2023
1359-4311/© 2023 The Author(s). Published by Elsevier Ltd. This is an open access article under the CC BY-NC-ND license (http://creativecommons.org/licenses/by-nc-nd/4.0/).

Nomenclature

The following abbreviations are used in this manuscript:

CFD	Computer fluid dynamics.
CO	Carbon monoxide.
DISI	Direct injection spark ignition
ECN	Engine Combustion Network.
ECU	Engine Control Unit.
EGR	Exhaust Gas Recirculation.
GDI	Gasoline Direct Injection.
NOx	Oxides of nitrogen.
PN	Particulate number.
ROI	Rate of injection.
ROM	Rate of momentum.
Rp	Ratio of saturation to ambient Pressure.
SOE	Start of energizing.
SOI	Start of injection.
THC	Total hydrocarbon.

considered a non-flashing regime, $3.3 > R_p > 1$ is for a transitional regime, and, when the $R_p > 3.3$ the condition is considered as strong flashing condition [9,10]. The flash boiling intensity can be controlled by varying the ambient gas pressure, fuel temperature, and saturation vapor pressure of the fuel, this last one depends on the fuel utilized.

$$R_p = P_{sat}/P_{amb} \quad (1)$$

Combustion under flash boiling conditions has shown potential benefits for homogeneous lean combustion at high load [11,12], which is a beneficial engine operation mode for reducing the fuel consumption and lowering the oxides of nitrogen (NOx) [13]. On the other hand, these sprays in combination with other strategies, have shown significant improvement in engine performance. For instance, combining flash boiling spray under lean-burn conditions with split injection strategies has resulted in higher combustion efficiency and less total hydrocarbon (THC), carbon monoxide (CO), particulate number (PN), and NOx emissions compared to single injection and subcooled conditions [14,15]. Results show that, under flash boiling conditions, the droplet velocity significantly increases while the droplet size reduces [16,17]. Chang et al. [17] also concluded that mild flash boiling is preferred over subcooled conditions.

The spray collapse phenomenon, which occurs in gasoline sprays because of its high volatility and the particular conditions during which the fuel is injected, is another process that is still a topic of extensive research. Spray collapse can be induced by flash boiling, and also be enforced in non-superheated conditions by increasing the flow hole number of multi-hole injectors. The collapse depends not only on the operating conditions but also on the fuel properties, as it was found by Aleiferis and Van Romunde [18] when comparing ethanol and butanol, as well as other authors [19,20]. Li et al. [21] encountered that the collapse of multi-jet flash-boiling sprays was induced by vapor condensation at the nozzle exit. In all cases, plume-to-plume interaction plays a major role [10,20].

Thermo-physical properties of the fuel, such as saturation temperature, latent heat of vaporization, surface tension, density, and viscosity, are the key parameters to determine the atomization and evaporation processes [7]. Numerous types of hydrocarbons compound gasoline, therefore, it is not easy to precisely reproduce the same gasoline composition for research purposes. Typical gasoline surrogates have been Isooctane/Heptane mixtures which goal is to simulate the octane number to control the degree of auto-ignition. Although they are suitable for combustion, they fail to replicate the gasoline volatility when studying flash boiling, in which the volatility factor is crucial [22]. For example, in several studies, Isooctane liquid penetration was significantly lower than other components, such as alcohols or short-chain components for the same condition [7].

Yan et al. [23] studied the spray shape for Isooctane, Hexane, and ethanol, through lateral Diffuse back-illumination (DBI), finding that the spray shape changes depending on the flash boiling intensity. Adding volatile components, like Hexane, into less volatile fuels could lead to stronger flash boiling under the same ambient pressure. On the other hand, Zhao et al. [24] found that Pentane has the most considerable aerodynamic breakup level, which helps to increase the flash boiling intensity in gasoline sprays.

It has been shown that flash boiling sprays' morphology changes abruptly when the spray collapses, and classical parameters of spray angle and penetration do not fully describe it [9,25,26]. The radial expansion of the spray has been used instead for the flashing sprays to better comprehend the phenomena taking place. Other authors have employed different approaches such as, Du et al. [10] who used the front view Mie-scattering technique to introduce a new criterion, named spray collapse percentage, to determine the spray collapse regime by dividing the area of spray region calculated by a pre-defined circle.

Finding better simulation models that can encompass all the features of such volatile and changing sprays remains challenging [27]. In this sense, augmenting the data available is the best path to further comprehend the processes involved in the spray and develop more accurate models, for which optical diagnostic tools have been of crucial value [1].

The works carried out by [9,10] present methodologies and approaches similar to different sections of this article by studying the radial expansion of the spray and its frontal view, however, in one case, the experiments were done at an injection pressure of 100 bar (10 MPa) for only one fuel surrogate. Besides, there are only a few articles with injection temperatures higher than 90 °C. Furthermore, most works [25] have analyzed classical parameters to qualitatively describe the spray morphology under non-collapsing conditions, but there are still pending tasks on quantitatively characterizing this phenomenon.

This study aims to shed light on the different collapse types present in a GDI spray, for different gasoline components ranging from low to high volatiles, covering injection temperatures up to 120 °C, more similar to those of an actual GDI engine. This allows us to analyze a broad range of R_p values. Further, in addition to studying the radial expansion for different conditions, a new method to describe the collapse from frontal images is shown. The approach consisted of observing the central area of the spray over the injection event, taking special attention to the moment when the nozzle tip is clouded by the spray, meaning that the jet plumes have collapsed into a single one. From the results obtained, indices to quantify the collapse instant, as well as to correlate quantitatively the degree of collapse to the injection conditions are introduced. Understanding and predicting the instant when the collapse occurs helps to better inspect the injector's ideal design strategy and increase fuel use effectiveness. In this sense, this work condenses novel approaches to identify, analyze and quantify the spray collapse using several fuels and more real injection conditions.

2. Materials and methodology

2.1. Test rig and injection conditions

The facility used has three wide windows for the light path. The test rig was built to uphold under-pressures and pressures ranging from 0.01 bar to 15 bar, that simulate those of an actual engine, especially, early injection conditions. The chamber temperature is controlled by supplying nitrogen from below the chamber in which a heater module is placed. This module consists of a 2 kW resistor, an air diffuser and its casing. Thanks to this, the vessel is able to reach up to 150 °C. The gas used to pressurize the chamber was nitrogen. A render of the chamber

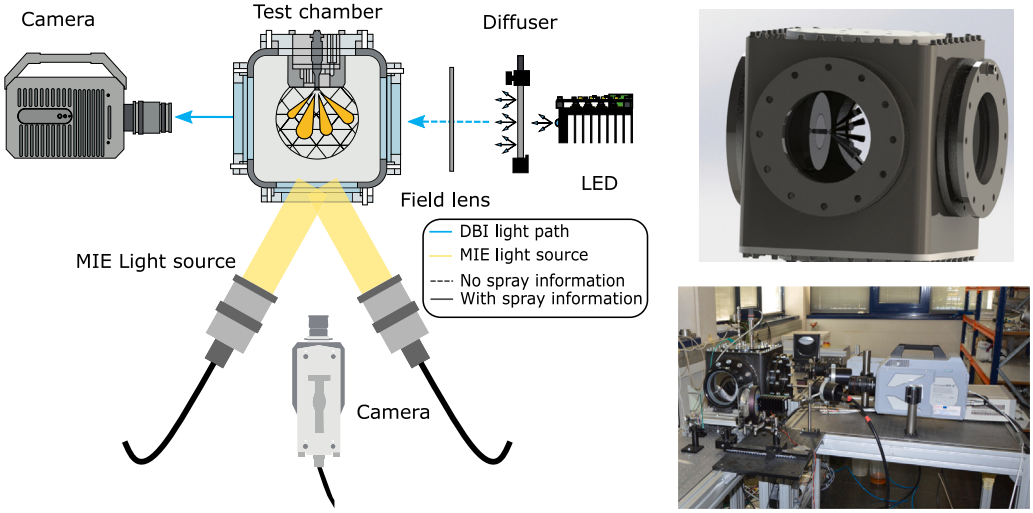

Fig. 1. Diagram of the optical setup on the GDI test rig.

can be seen in the right side of the Fig. 1, and a thorough description of it can be found in [22]. The injection temperature is controlled by a thermoregulator unit which passes oil in a closed loop through a special injector holder that allows the oil to reach the nozzle.

2.1.1. Injection system

The fuel was delivered through a high pressure pump connected to an electrical motor. The fuel exiting the pump first reaches a common rail before going through the high pressure line to a second 12.3 cm^3 rail. The fuel pressure is controlled by an electrically actuated valve. Finally, the fuel reaches the injector which is electrically actuated by its own ECU (Engine Control Unit). A Spray G injector from the ECN network which has been widely used for research purposes was employed; the injection duration was controlled by a TTL signal following the ECN recommendations [28].

Fuels employed

Four fuels were used to study the effects of flash boiling and spray collapse on the spray morphology during gasoline injection. The fuels were chosen to emulate the gasoline volatility and provide more extreme cases of flash boiling. Besides, the fuels are mono-component, providing a more straightforward starting point for computer fluid dynamics (CFD) modelers in the future. The conditions measured were selected based on the ECN [28]. Furthermore, mild and strong flash boiling conditions points were pursued using fuels' vapor–liquid phase diagram. The conditions investigated are represented in Fig. 2 as black points. The commercial gasoline fuel RON98 vapor pressure curve extracted from [29,30] is only shown for comparison purposes and the vapor and liquid phase labels refer to the main state of the fluid at those specific conditions. As it is natural for multi-component fuels, the curve position varies depending on the fuel composition, which changes depending on the seasons and even among fuel batches delivered to gas stations. From the Figure, the Hexane is the closest to gasoline in the vapor pressure curve as well as in volatility which are the leading parameters for the flash boiling phenomena. This allows us to contrast how the spray morphology changes in Gasoline, to some other mono-component surrogates that are often chosen due to their octane number and other combustion properties. The conditions tested are also depicted in Table 1.

The most relevant properties of each fuel are showed in Table 2, being the Hexane the fuel with the closest vapor pressure curve to the commercial gasoline from Huang et al. [29] and [30].

Table 1
Test matrix for visualization experiments.

Parameter	Value/Type	Units
Fuels	Isooctane/Heptane Hexane/Pentane	
ET	0.68/1.2	ms
Rail pressure (P_r)	200	bar
Back pressure (P_b)	0.2/0.5/1/3/6/15	bar
Fuel temperature (T_{fuel})	20/60/90/120	°C
Ambient temperature (T_{amb})	20/90	°C
Repetitions per test	10	

Table 2
Fuel properties obtained from the National Institute of Standards and Technology (NIST) [31].

Properties (@300 K)	Pentane	Hexane	Heptane	Isooctane	Units
Liquid density	618.8	652.84	677.81	696.57	kg/m^3
Viscosity	0.214	0.291	0.376	0.456	$mN\ s/m^2$
Surface tension	15.25	17.73	19.82	20.96	mN/m
Vapor pressure	73.57	22.01	6.72	2.08	kPa
Latent heat	35.1	31.1	36.3	41.4	kJ/mol
Specific heat	2.34	2.26	2.24	2.04	kJ/kg K

2.2. Optical techniques

Visible light-based techniques have been the standard for studying rapid phenomena like liquid injections. Thanks to the numerous advantages provided by these non-intrusive techniques, they are applied to acquire images of the liquid phase of the spray. Ten injection cycles per test point were recorded. The conditions varied in order to cover a broad variety of flash boiling and spray collapse conditions.

In this work, an arrangement of two optical techniques is utilized for the simultaneous estimation of the liquid phase of the spray from a lateral line of sight (Diffused Back Illumination) and frontal side (MIE scattering). A similar configuration was also used by Du et al. [32].

2.2.1. Diffuse back-illumination

In DBI, the light is extinct because of the spray core and droplets' optical depth (τ). The technique has extensively been used in various studies [22,33,34]. A fast light-emitting diode (LED) is employed for illumination; this enhances the nature of the images acquired, using very short light pulses with the order of nanoseconds, with the exposure limited by pulse duration and not by the camera, resulting in sharper frames.

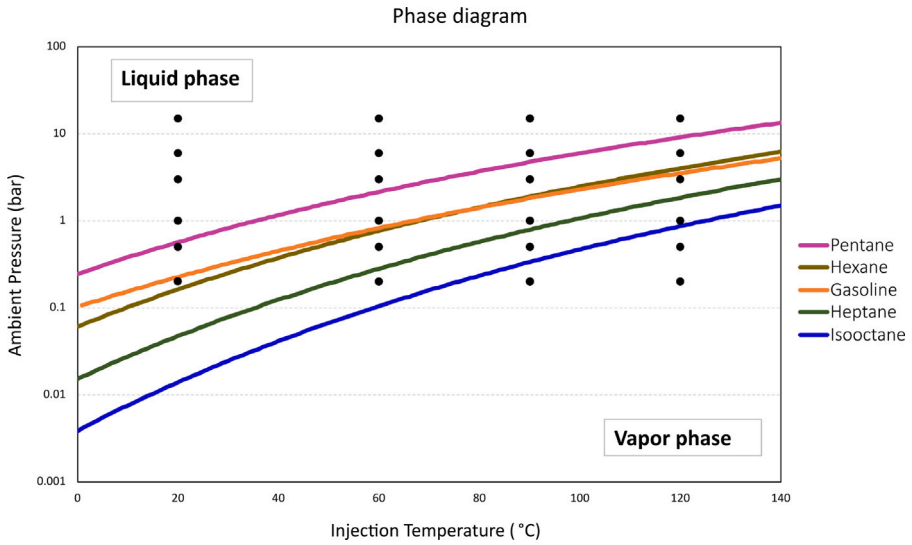

Fig. 2. Phase diagram of all the fuels. The experiment conditions are represented as points.

The extinction is calculated each instant using the Beer–Lambert law described in Eq. (2) [35]:

$$\frac{I}{I_0} = e^{-\tau} \tag{2}$$

where I is the intensity of the frame taken into account attenuated by the spray and I_0 is the reference image from the source without attenuation.

The DBI optical improved setup used in the experiments was first introduced by Ghandhi and Heim [34] and is shown schematically in Fig. 1. It is composed (left to right) of the LED light source, diffuser, field (Fresnel) lens, and a high-speed camera on the other side of the test chamber. Then, a 100 mm diameter engineered diffuser with 20.5° divergence angle is used to homogenize the light. Next, a Fresnel lens with a focal length of 67 mm was employed to replicate the diffused light source at the optical plane of interest of the spray. A blue LED is combined with a blue filter before the camera lens allowing to reduce the light interference from another optical setup measuring at the same time, resulting in a much clearer captured image. The blue LED unit used was composed of the control circuit, heat sink, and a parabolic reflector in order to reduce the LED light aperture from 120° to 25°, concentrating and reducing light loss. Images obtained through this technique are later showed in Fig. 4.

2.2.2. MIE scattering

Mie-scattering (MIE) is an optical phenomenon named after Gustav Mie. It refers mainly to the elastic scattering of light from atomic and molecular particles whose diameter is larger than about the wavelength of the incident light. MIE phenomena can be used in liquid spray investigation since the liquid droplets of the spray reflect the incident light [36]. The MIE setup employed in the experiments is illustrated in Fig. 1. Two Mercury-Xenon arc lamp light sources are used. The light is transported using optical fiber to a 7 mm diameter collimator lens that permits concentrating the light in the region of interest. This light is scattered back differently by the spray and the vessel wall in the background, then collected by the camera for appropriate processing.

2.3. Image processing

One essential step in any visualization experiment is the image treatment to extract as much information as possible. These optical techniques imply that the fast cameras record a video in which each frame is processed separately as an independent image. The methodology utilized in this work has been thoroughly detailed in previous works [22,37], and here only a brief explanation is presented.

There are four main steps to process each frame: image masking, background subtraction, contour detection, and contour analysis.

Initially, the frame is **masked** by selecting the overall part of the image where the spray will be, discarding other areas such as the injector holder, windows' limits, etc. Then, **the background is subtracted** from the image, leaving only the spray. This step is carried utilizing Eq. (2) where the optical thickness is calculated, being I_0 the image of the background before the injection event, and I the image containing the spray.

Later, **the spray contour is differentiated** applying a fixed threshold for image binarization (background - spray). The threshold was adjusted to fit better the contrast given by each optical technique, and once defined, kept constant for the whole experimental campaign. Additionally, the image is filtered through morphological image operations such as dilation and erosion, removal of noisy pixels, etc. For the background average, seven frames before injection were used. Finally, **the contour analysis** can provide important parameters like spray penetration, angle, width, etc [38,39]. Further, the start of injection (SOI), calculated by extrapolating the penetration curve to zero [38,40], was gotten to phase the time domain of the results and better compare the test points. A image depicting the contour differentiated after the steps mentioned is shown in Fig. 3. The Spray pattern in the left can be approximated to a triangle, whilst, to the right there is a spray collapse due to the high density, the shape is more rounded and asymmetrical.

2.4. Spray collapse processing approach

For flashing conditions, when the pressure of the chamber is lower than the vapor pressure of the fuel at its injection temperature, the spray structure suffers several changes that are difficult to describe only with classical parameters of penetration and angle as other works have tried [9,41], so a deeper analysis of the contour is required.

Figs. 4 and 5 illustrate some of the changes in the spray morphology at different injection conditions at the same time step. Each subfigure is a snapshot (at t = 0.5 ms after SOI) that can be used to describe the spray cone formation qualitatively. An $R_p > 1$ indicates that the spray is under flashing conditions, and it is shown at some of these conditions that there is a collapse of the sprays.

Previous works have been trying to characterize the level of flash boiling at each particular injection condition through the R_p number; however, it has been observed that this variable does not always describe the spray morphology [42,43]. Therefore, R_p is an indicator of flash boiling but not spray morphology such as spray collapse. For

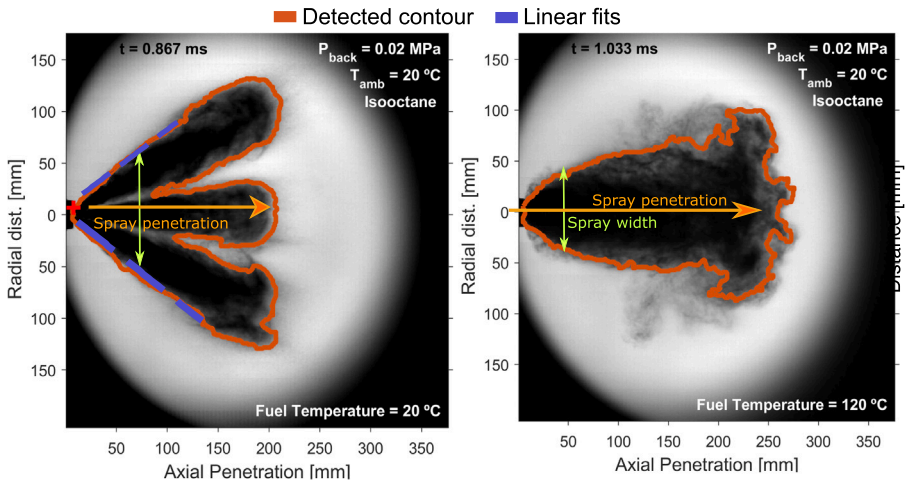

Fig. 3. Macroscopic spray parameters extracted from the contour analysis. Two structures are seen for non-collapsing (left) and collapse sprays. The conditions are depicted on the image.

example, in Fig. 4 it is observed that for similar R_p (0.07 and 0.058), the spray morphology is different, and that for $R_p > 1$ there is no collapse.

In this sense, the spray is analyzed by means of the spray width when the spray is fully developed. After the contour is differentiated, the distance between the upper and lower limit of the spray is calculated for each axial distance; then, all ten repetitions are averaged (Fig. 3).

The spray width variation along all injection conditions is analyzed to see how the different flash boiling regimes affect the spray morphology.

2.4.1. Nucleation rate correlation to jet width

The radial expansion of a flashing spray jet near the nozzle exit is highly influenced by the mixing of the vapor phase in the two-phase flow and is limited by the ambient gas [44,45]. In this sense, another approach in the literature to correlate the jet width with the flashing phenomena is by introducing the nucleation rate [45]. Thus, parameters influencing the vaporization rate and discharge ambient resistance are relevant. The nucleation rate (J) can be expressed as:

$$J \propto \sqrt{\frac{2\sigma}{\pi m}} exp\left(-\frac{\Delta G^*}{k_B T_{fuel}}\right) \tag{3}$$

where m is the molecular weight, ΔG^* is the free energy barrier, σ is the surface tension, and finally, k_B is the Boltzmann constant [42,46]. Since the start of the vaporization is caused by homogeneous nucleation in the internal flash boiling jet [47], the free energy barrier for homogeneous nucleation could be represented by Eq. (4) [48].

$$\Delta G^* = \frac{16\pi v_l^2 \sigma^3}{3k_B^2 T_f^2 \ln^2(R_p)} \tag{4}$$

where v_l is the specific volume of liquid, which is defined as:

$$v_l = \frac{m}{\rho_l N_A} \tag{5}$$

Being Na the Avogadro number. In this work, the range of experimental conditions is mostly influenced by the exponential term of Eq. (3). Consequently, the exponent, called from now on X presented in Eq. (6), is used as an indicator of the nucleation rate.

$$X = \frac{\Delta G^*}{k_B T_{fuel}} \tag{6}$$

Rate of vaporization vs spray width

A relation of the rate of vaporization with the spray cone width is presented. It can be done through the phase change chemical potential (Eq. (7)), which is denoted as $\Delta\mu$ as explained in [49].

$$\Delta\mu = \mu_{liquid} - \mu_{gas} \tag{7}$$

Assuming that the flash boiling injection event is an iso-thermal process [8], the Maxwell relation to represent the chemical potential is shown in Eq. (8).

$$\left(\frac{\delta\mu}{\delta p}\right)_{T,n} = \left(\frac{\delta V}{\delta n}\right)_{T,p} = v \tag{8}$$

Being v the specific volume. v is defined for ideal gas and liquid phases as shown in Eqs. (5) and (9).

$$v_g = \frac{RT}{P} \tag{9}$$

Being R the ideal gas constant. Then, combining equations it could be obtained an expression for the chemical potential difference, depicted in Eq. (10).

$$\Delta\mu = RT_{fuel}\ln\left(R_p\right) - \frac{M}{\rho_l}(P_{sat} - P_{amb}) \tag{10}$$

3. Results and discussion

3.1. Spray width

The spray width is a good approach to describe the spray morphology at different conditions. For each time step it can capture the instantaneous spray shape. The results obtained when plotting the spray width for each axial position are depicted in Fig. 6 comparing the different nozzle temperatures studied for the same fuel. The figure depicts the results for Isooctane and Hexane. Since Hexane is a more volatile fuel with higher R_p for the same injection conditions, the collapse starts taking place at 60 °C, which for Isooctane happens at 90 °C. The collapse is identified by observing the width change, when the slope is not constant or changes in relation to a linear one, it means that the angle of the spray has decreased, and consequently, started to collapse.

Three different spray patterns are identified in the plots located in the upper row of the figure. A frame for each pattern are shown in the lower row. The first one corresponds to the 120 °C (both fuels) and T = 90 °C (Hexane). Here, the R_p relations are the highest, therefore, there is a strong flashing condition that clearly shows a collapse of the sprays. The second pattern is for T = 90 °C (Isooctane), and T = 60 °C (Hexane), which depicts a mild collapse of the sprays. Note that the profile of the first axial 20 mm matches for the two patterns. From that point onward, the width increases due to big vortices appearing thanks to the resistance to the spray advance since its cone has not fully collapsed [6,50]. The third pattern is seen for non-flashing conditions (R_p < 1). The line possess a fixed slope which represents a constant spray cone angle, hence, not collapsing.

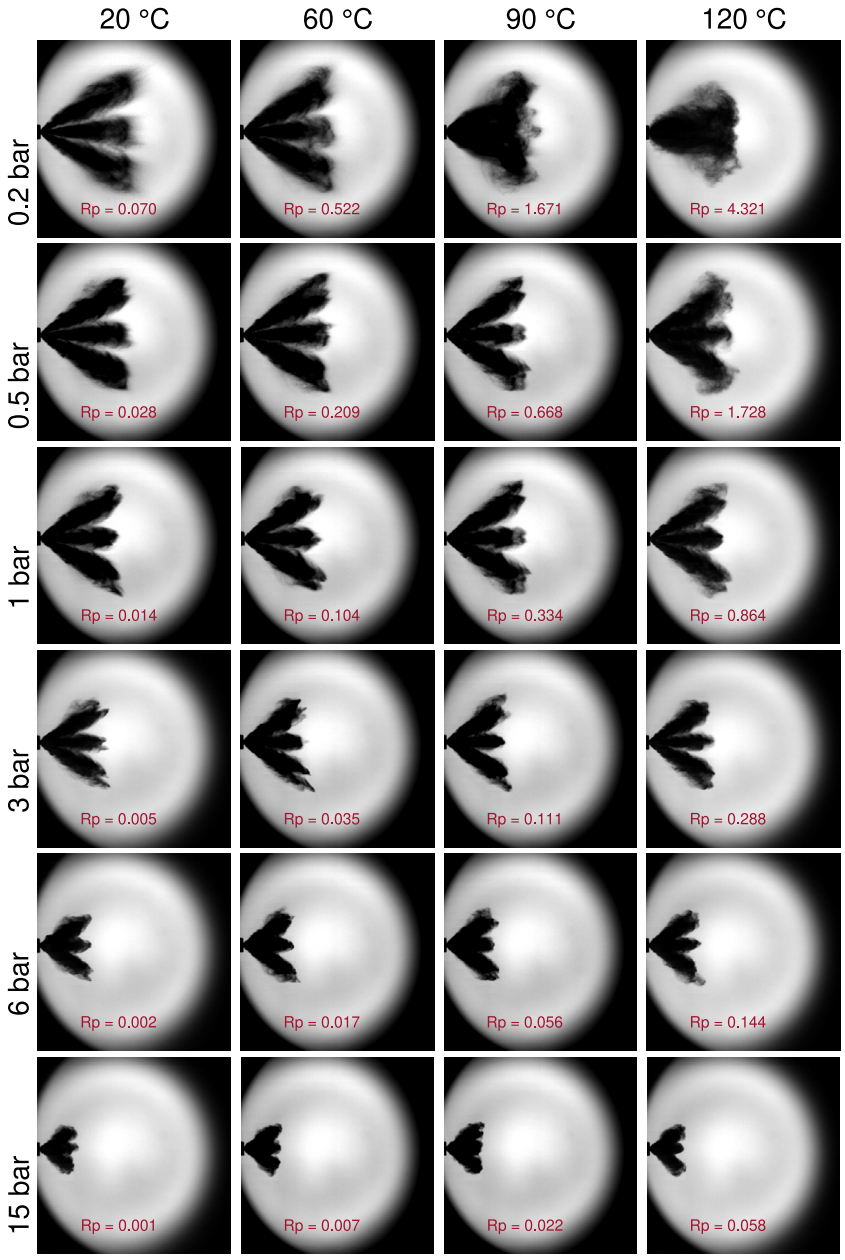

Fig. 4. Spray cone morphology for Isooctane in Spray G injector.

If the first 15 mm are zoomed, different width curves for the collapse and non-collapse sprays can be observed as shown in Fig. 7 for Isooctane. From the very first millimeters from the nozzle, the flashing conditions (T_f = 90 °C and T_f = 120°) yield different width curves. Moreover, it is noted that the curve's nature is different for them which could be approximated to a log equation for the first millimeters, whereas for the non-flash boiling conditions, it is likely to fit on a linear curve. For the latter case, it could be that momentum diffusion is playing a major role in the radial expansion, which for flashing conditions is the rate of vaporization the leading phenomena as discussed in Section 2.4.1.

Finally, if we compare the fuels in one plot, since the same test conditions would provide different R_p values, the more volatile fuels have the more severe flash boiling conditions. Fig. 8 depicts a condition in which the spray structure is very different because of fuel properties. In this case, three assorted spray structures can be found: the Isooctane and Heptane curves indicate non-collapse structures, whereas the Hexane and Pentane curves show two different spray structures with varying degrees of collapse. These changes are presumed to be due to the level of flash boiling, influenced by each fuel volatility, since, when plotted, all fuels presented the same liquid penetration during the injection [22] and from Weber and Reynold number estimation, the atomization regimes for the conditions tested were the same [51].

3.1.1. Spray collapse identification

Now that differences are evident for the stabilized jet in Fig. 6 for different collapse regimes, each condition can be differentiated from the non-collapse curve. Initially, each spray width is normalized, taking the condition with the nozzle temperature of 20 °C as reference (No spray collapse) along the axial distance for each injection condition to detect when the spray has collapsed.

After normalization, a more extreme contrast is detected for the collapsing curves. If the variation with respect to the reference line is averaged, the mean values belonging to collapse images present a higher deviation from the reference (see Fig. 9(a)). If all these deviations for all fuels are plotted against R_p, a clear trend should be formed,

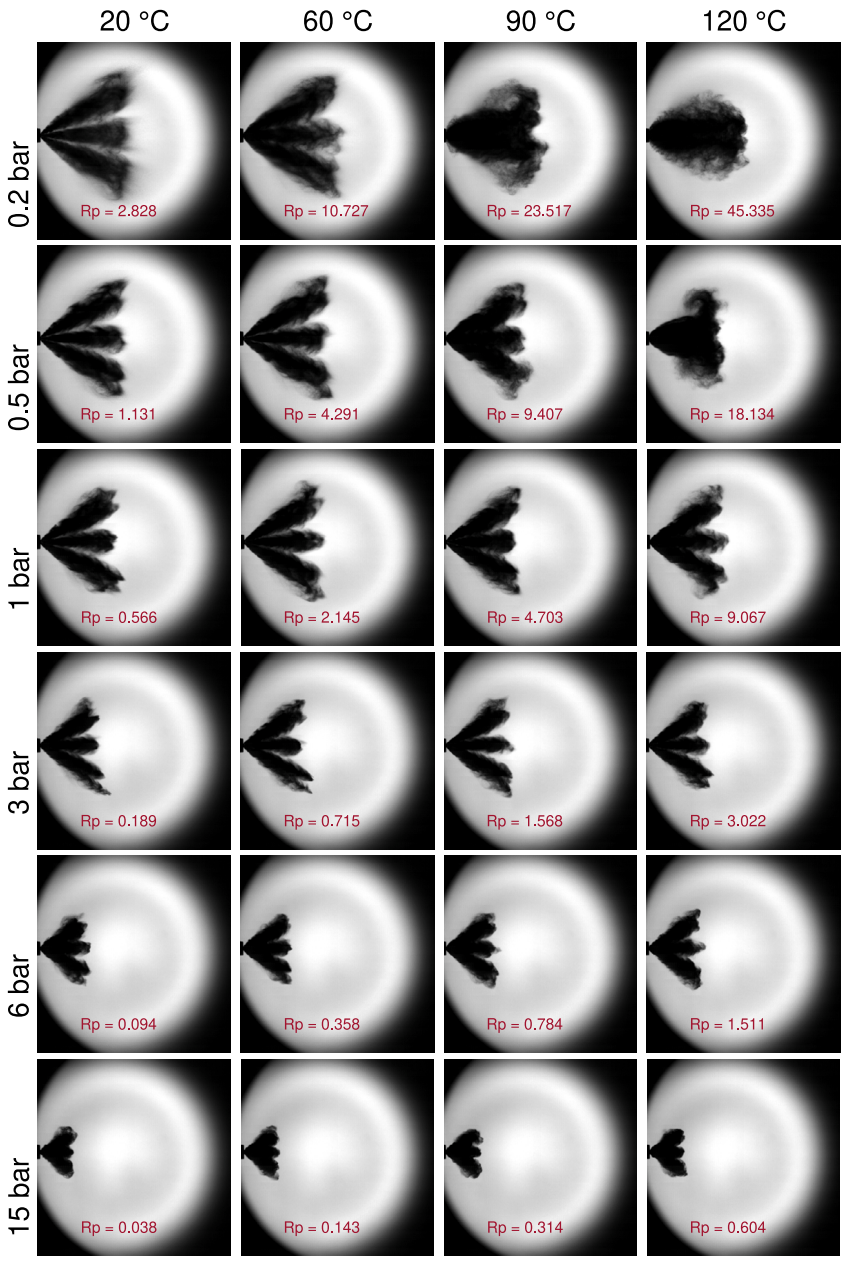

Fig. 5. Spray cone morphology for Pentane in Spray G injector.

in which, for lower R_p all sprays should be non-collapsing; while for higher R_p the separation should increase. This trend is effectively found, as shown in Fig. 9(b), then, this deviation can be correlated to the degree of collapse. Also, a cloud of points is found with minimum variation to their reference. From this concentration of points, we can extract and refine iteratively a threshold to separate and identify the non-collapsing conditions. The threshold is adjusted by plotting a histogram of the deviation (bin = 0.25 mm) in which the cloud of points is separated from the rest. From there on, mild or transitional collapse appears up to strong collapse conditions, for which threshold is determined using the same histogram; however, the limit is not as evident for the data used, and the selection was made when the higher gap in the histogram was encountered.

The threshold for this data set was found at 3.25%, at R_p close to 1.5 for the transitional collapse to begin (see Fig. 9(b)). Strong collapse conditions start at R_p near 3.7 with the threshold selected at 19%. An example of the classification of the collapse conditions is given in Fig. 9(a) legend.

3.2. Radial expansion of the jet

Fig. 10 shows the relation between R_p and width at two axial distances from the nozzle tip based on the orifice diameter, d. It is shown the width for 5d and 20d. The width increases with R_p in general, especially at flashing conditions ($R_p > 1$). The increment is more noticeable for the most volatile fuels, i.e., Hexane and Pentane. Note that at highly flashing sprays ($R_p > 3.5$) the trend is not as clear as for lower R_p. Probably at those high R_p, the mechanisms that produce spray collapse are starting to affect the spray width. On the one hand, the flashing sprays produce a radial expansion of the jets; however, the choke of the air entrainment due to the jet expansion (spray interaction) creates the inner low-pressure zone that attracts the sprays [6,21]. Thus, there are effects that could counteract each other to some extent. Guo et al. [45] also reported this behavior when analyzing the radial expansion for Hexane, stating that R_p lacks generality in describing the radial expansion.

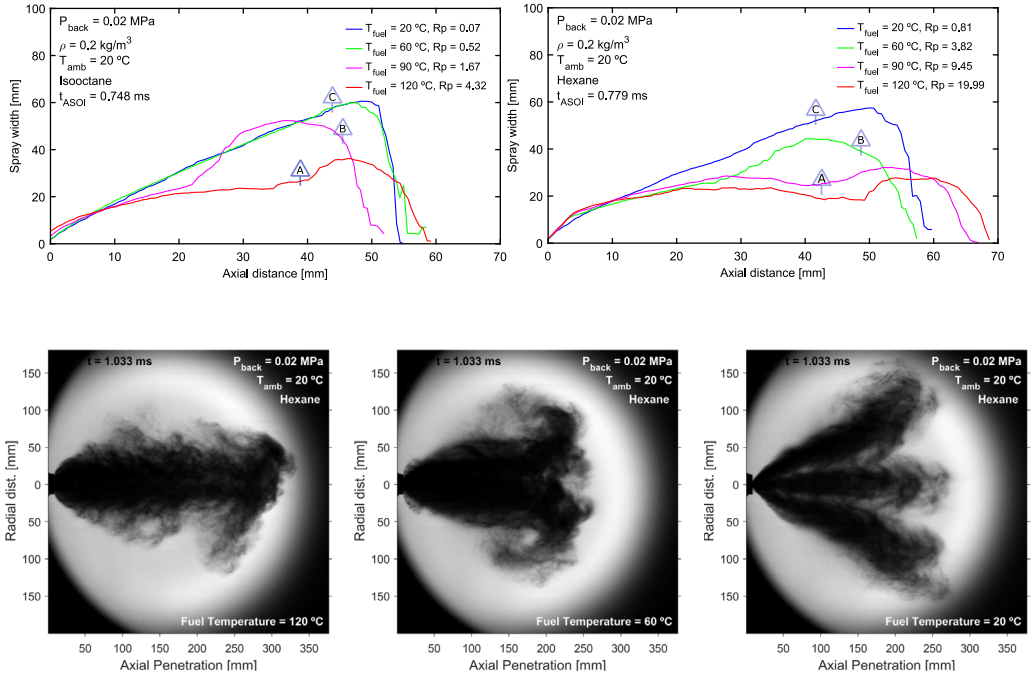

(a) Collapsing condition (b) Mild collapsing condition (c) Non collapsing condition

Fig. 6. Liquid spray width for different fuel temperatures for a time when the jet has fully developed. Two out of the four fuels tested are shown. Also, different collapse structures can be seen. All injection events occur at 200 bar of injection pressure.

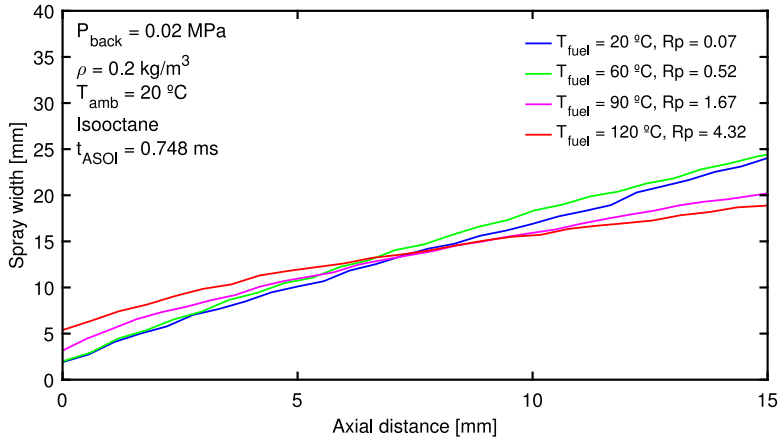

Fig. 7. Zoomed liquid spray width of Spray G injector for different fuel temperatures.

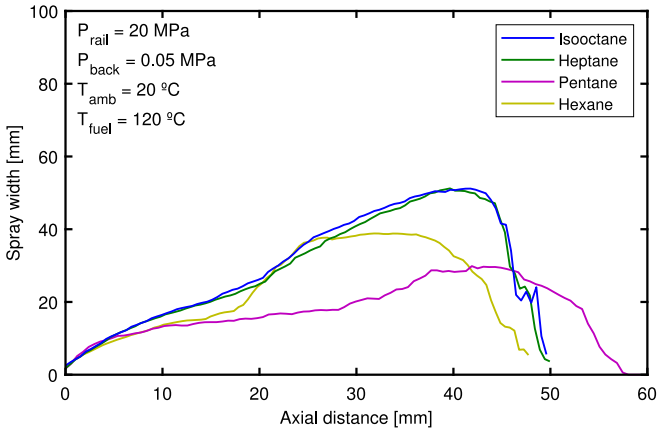

Fig. 8. Liquid width for the different fuels used.

3.3. Radial expansion of the jet by nucleation rate

Fig. 11 reports the relation between the X parameter and the cone width of the Spray G injector and only two distances are shown. For a better display, the cone width is plotted against $X^{-0.5}$. Moreover, to account for the drag effects of the discharge gas density [52,53], the $X^{-0.5}$ is multiplied by $P_b^{-0.5}$ (ambient pressure). It is observed that there is a generally weak relation between the two parameters, at least much weaker than with R_p. Thus, there is no clear relation between the width and the nucleation rate, despite the isooctane, which shows a certain trend for $20d_0$.

A possible cause is that the spray expansion is reliant on the flow state at the nozzle exit. According to Chang et al. [6] and Park and Lee [54], at the internal flashing regime, there is already a two-phase flow developed inside the nozzle. The nucleation process occurs at the start of the phase transition; which, in this case, it would be before the spray exits the nozzle, hence, reducing the nucleation rate impact on the observable jet expansion, being then the rate of vaporization a more

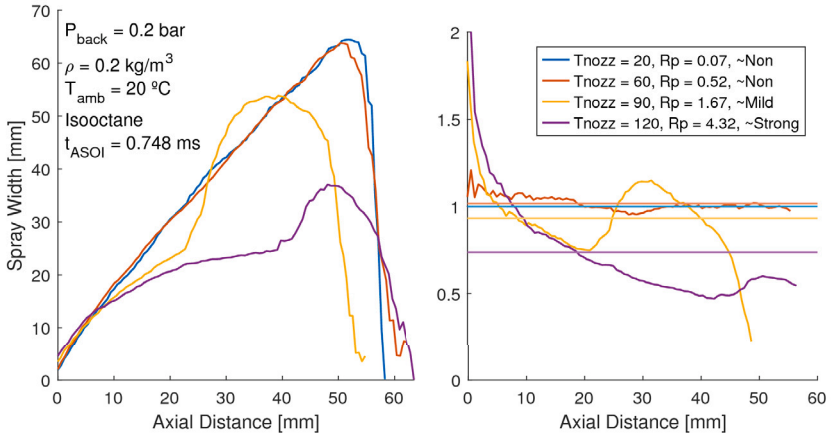

(a) Identifying spray collapse for Isooctane. Horizontal lines are the mean average of the variation.

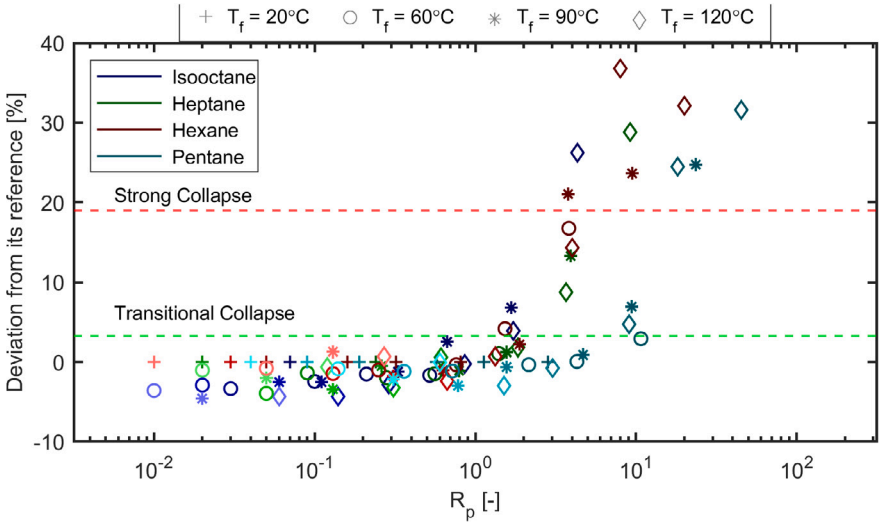

(b) Instantaneus variation vs R_p. Dashed horizontal lines mark the limit for transitional and strong collapse. Injection conditions can be found on the Figure.

Fig. 9. Spray Collapse detection based on width normalization parameter.

important variable [9]. Moreover, the counterbore nozzle geometry employed promotes air entrainment, which favors the occurrence of two-phase flow at the nozzle exit. Additionally, the flow radial velocity at this location increases, benefiting the spray breakup and atomization [55,56]. The air entrainment has also been shown to affect the transient behavior of the spray collapse and plume merging [57].

3.4. Vaporization rate

Fig. 12 shows the relation between the chemical potential, $\Delta\mu$, and the width of the spray. The parameter is multiplied by $T_f^{-0.5}$, which provides better visualization and relation to the spray cone width values. It can be observed that, in general, all fuels follow a similar trend to the one shown with the R_p plots; however, for $\Delta\mu > 1$, which is indeed at flashing conditions, it is shown an increment of cone width for all distances except to 60 d_0. According to Vetrano et al. [58], the flash boiling phenomena last at least 20 d_0; thus, for further distances, the width may not be wholly related to the jet flashing nature, which in the present case is from 40 d_0. It is likely that from that distance onward, other causes, like aerodynamic forces due to gas–liquid interaction and the onset of spray collapse, could play a major role in the spray cone width.

3.5. MIE frontal view analysis

The frontal perspective of the spray gathered through the MIE, identifying individual jets, allows to visualize the moment in which they collapse. As the injection develops, the different types of jets can be differentiated by monitoring the path followed by the jet and how it changes in time.

3.5.1. MIE frontal surface

The first analysis performed for this frontal view is the study of the evolution of spray surfaces over time. The treated frame is sliced into eight pieces, one for each jet, in which the spray contour is analyzed. The algorithm does not count the nozzle tip, so the contour detection starts from a distance to the center or nozzle axis. Fig. 13 shows three different test conditions for Isooctane for the same time step. For the P_b = 0.2 bar, as the fuel temperature changes, it is shown different flashing conditions. For T_f = 20 (left image), the R_p is 0.07, so the spray is not under flashing conditions. For T_f = 90 and 120 (center and right images), the spray is under flashing conditions (R_p = 1.67 and 4.32 respectively), and it is observed how the spray morphology and surface detected changes.

The spray cone structure is altered at the most extreme flash boiling events. The ultimate fuel distribution is concentrated in the borders

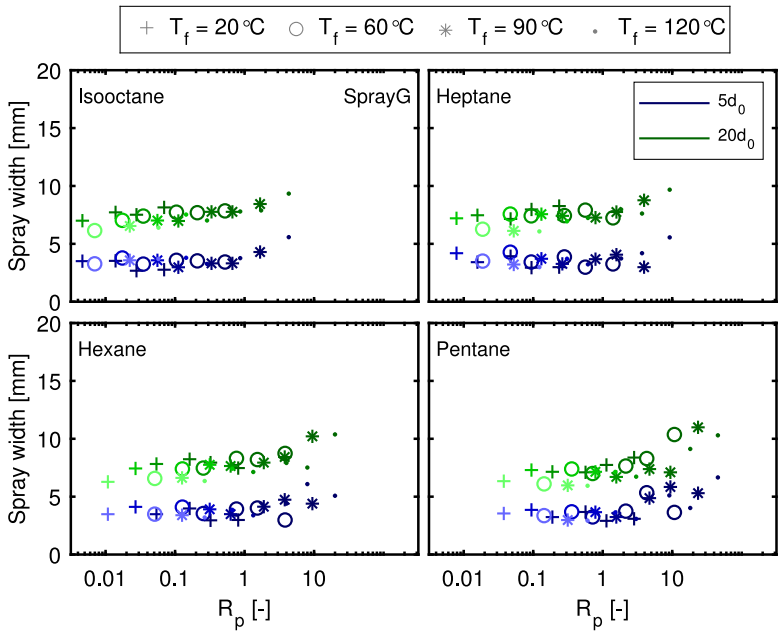

Fig. 10. Width vs Rp, for all the fuels tested on SprayG injector.

between the jet and its neighboring jets as a result of the spray plumes' significant expansion and interaction. Therefore, the fuel is concentrated in areas where there would not be spray for a regular injection. This occurrence appears in the right image of Fig. 13.

If all the individual jet surfaces are added together for each frame, it could be obtained the evolution of the frontal projection surface over time. The growth or decrease of the surface detected is related to the amount of fuel liquid phase projected on the frontal view. It could also indicate, to some extent, the amount of fuel that could be evaporated or the advancement of the liquid phase. Fig. 14 shows the spray surface evolution over time. The left image (14(a)) depicts the surface for various back pressures. Note that as the discharge pressure decreases, the spray surface grows at a greater rate, because it allows for a faster sprays' fuel distribution in the chamber. Nonetheless, when it reaches a point of $P_b = 0.2$ bar, the tendency changes since it is under flash boiling conditions. The growth rate is different because of fuel evaporation but also due to spray collapse that concentrates the spray in the injector axis. In contrast, in other conditions, the fuel is pushed outside the field of view of the camera.

On the other hand, the right image (14(b)) reports the surface for different fuel temperatures at a discharge pressure of 0.2 bar. It is observed two major trends, the non-flash boiling cases (T_f = 20 and 60 °C) have a steep rise until the EOI at around 1.1 ms. From that point onward, the fuel moves out of the image and evaporates so the surface detected decreases. Contrary, for the flashing cases, there are two spray structures. One in which spray collapse occurs from the very beginning (T_f = 120 °C) due to the fuel concentration in the injector axis. The another one has a similar spray surface slope to the non-flashing cases, however, at some point diverges. In these collapse cases, the fuel concentration in the injector axis causes that even after the injection has ended, the fuel does not spread and remains in the center axis.

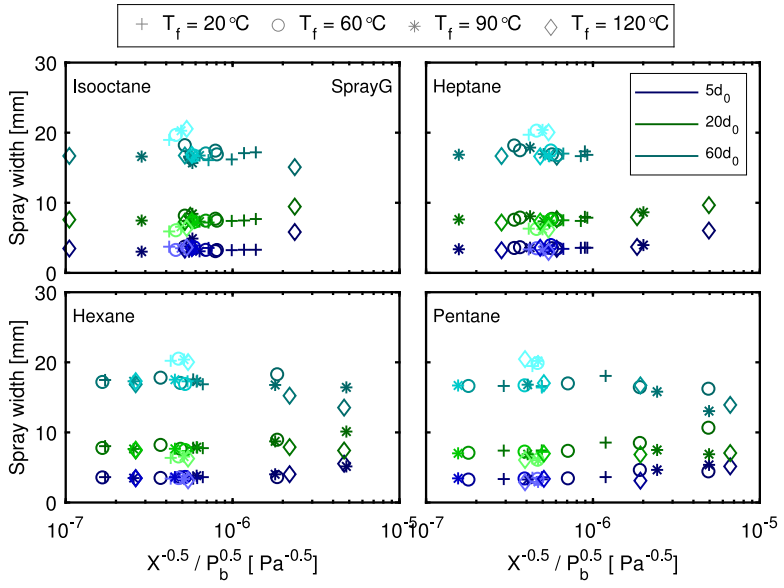

Fig. 11. Width vs X, for all the fuels tested on SprayG injector. Only two distances are shown for clarity purposes.

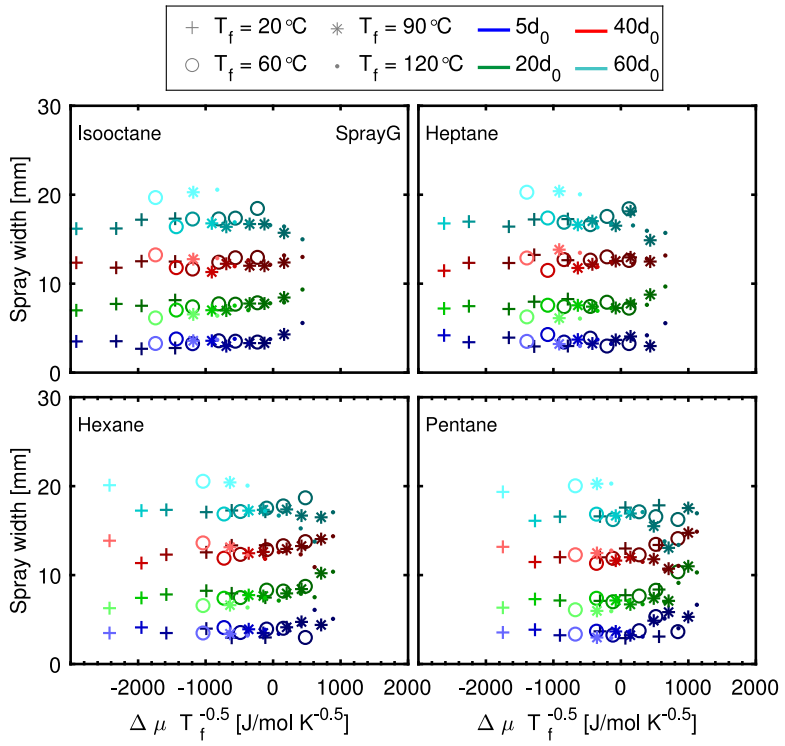

Fig. 12. Width vs $\Delta\mu$, for all the fuels tested on SprayG injector. For distances relatively close to the nozzle.

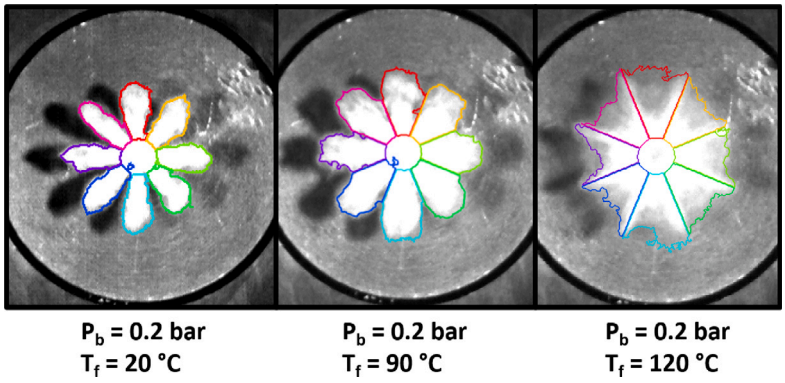

Fig. 13. MIE images for Isooctane, at a given time step (15), with the superposed contour of each spray. The captures represent diverse sprays structures due to flash boiling. From left to right, at T_f = 20 °C there is no flash boiling. The center image represents a mild flash boiling at T_f = 90 °C and the last image depicts strong flash boiling at T_f = 120 °C.

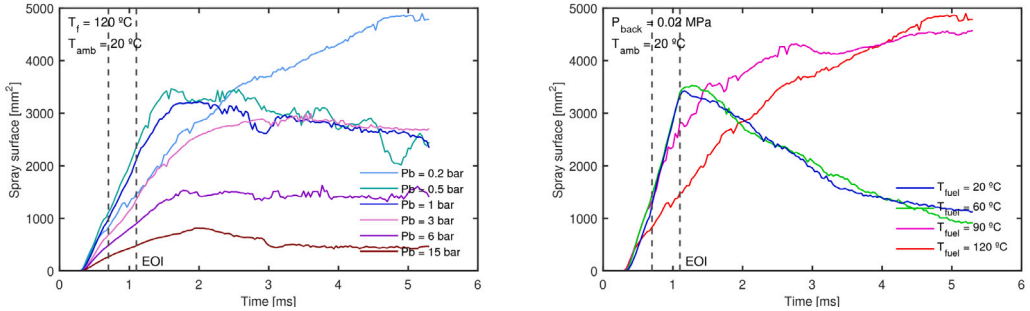

(a) Spray surface for different P_b. (b) Spray surface for different T_f.

Fig. 14. Spray surface against time for Isooctane.

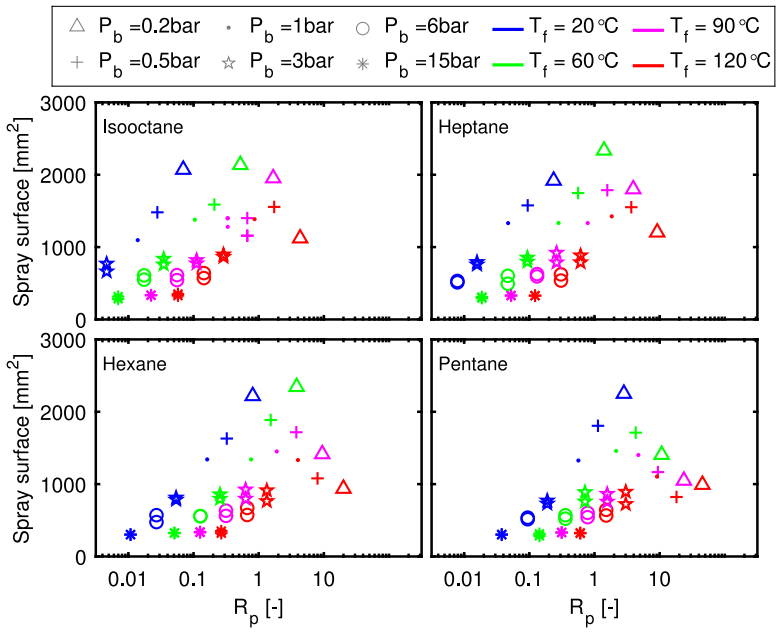

Fig. 15. Averaged spray surfaces at different R_p for each fuel tested. The color indicates different T_f.

For the injection durations tested, the surface values in which the spray is under the most stable conditions were selected just before the EOI. Fig. 15 represents an average surface value calculated between 0.7 and 1.1 ms (vertical dashed lines in Fig. 14) to condense all the test points. The surface values are reported against the Rp for each investigated fuel. A color is assigned for each fuel temperature, and each shape represents a different P_b. Lower P_b reported higher surface values, which is related to the lower ambient density and faster penetration of the spray [59]. It can be observed that there is a linear relation of spray surface with R_p for each temperature in all the fuels; however, at extreme flashing conditions $R_p > 3.5$, the surfaces stagnated or decreased. At these R_p values the spray collapses and changes morphology.

3.5.2. MIE collapse analysis through intensity monitoring

The collapse of the sprays into a single liquid jet due to flash boiling has been analyzed in the literature as a state of the developed spray [15,60]; nonetheless, there is some transitory mechanism that induces the spray collapse [21,50], thus, it could also be seen as a transitory phenomenon until it is fully developed. The approach aims to detect the moment at which the spray cone collapses. For this purpose, precise monitoring of the central area of the spray is performed over the injection event.

Fig. 16 shows the reasoning of the nozzle intensity monitoring. For the MIE images, the nozzle tip reflection was seen through all the injection events and only clouded by the fuel when the collapse occurred. Consequently, by observing the nozzle tip, some particular situations can be encountered.

On the right side of the Figure, there are three images of different injection conditions. Image #1 depicts a developed spray that is not under flash boiling conditions. Here, the white spot of reflection of the nozzle tip is visible throughout the whole injection. Image #2 shows a flash boiling test condition that has not collapsed yet, and it is possible to visualize the nozzle tip, despite having a $R_p > 1$. For Image #3, the spray is just about to collapse since the intensity levels for the nozzle tip are very low. Therefore, by monitoring the intensity levels of the pixels composing the nozzle tip (circled on the left side of Fig. 16), the time at which the spray collapses can be analyzed. Some principles must be taken into account here, the optical axis is aligned with the injector axis for this symmetrical jets' distribution. Besides, the camera focuses the nozzle tip since it is its intensity which is being monitored throughout the injection.

Fig. 17 depicts the time-resolved nozzle area average pixels intensities. Note that all the intensity values start at 0 since the background has already been subtracted. The 10 injection events are averaged to account for errors associated with shot-to-shot dispersion. The trend variability among injections was minimal which suggests that this method is robust and objective for its purposes of identifying the collapse instants.

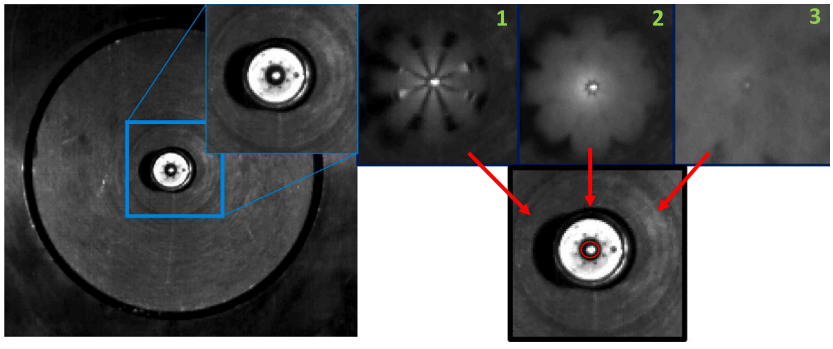

Fig. 16. Diagram of the nozzle tip intensity monitoring.

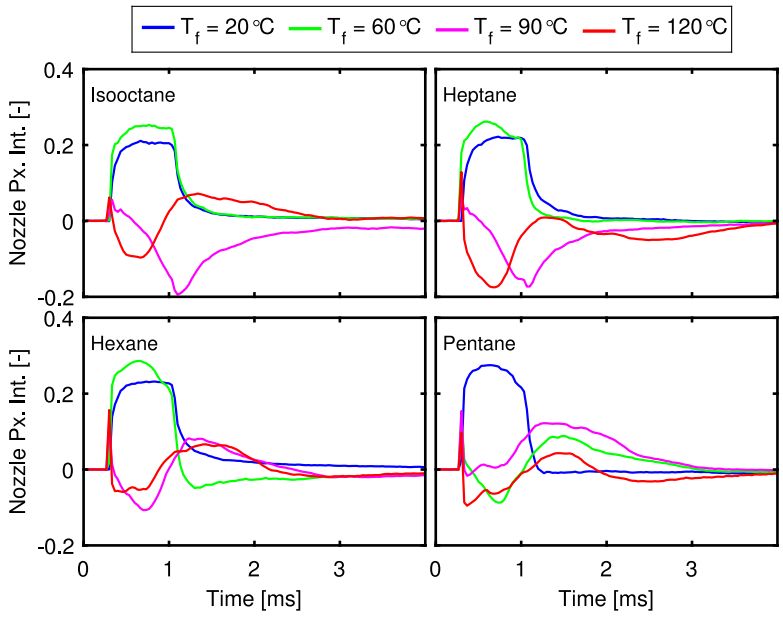

Fig. 17. Normalized nozzle area pixels intensity vs. time for the four fuels tested. Each color represent a fuel temperature. Test points shown are taken at P_b = 0.2 bar and T_{amb} = 20 °C.

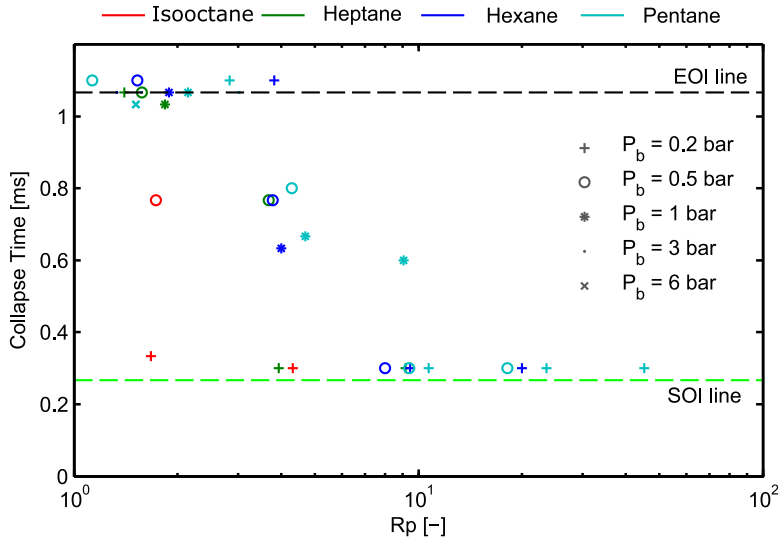

Fig. 18. Collapse time interpreted as the moment when the nozzle is clouded by the fuel versus R_p. Horizontal lines represent SOI and EOI.

This figure depicts the conditions of P_b = 0.2 bar with all the different fuels and fuel temperatures. As seen before, the fuel properties greatly affect the spray behavior. It is observed that three of the four temperatures for Hexane are collapsing, while on the other fuels, it can be noted only two. The Isooctane, for example, has two collapsing conditions at 90 and 120 °C. The nozzle pixel intensity values suffer a sudden increment at the start of the injection due to light reflection on the spray plumes that are starting to develop. Then, the rapid collapse decreases the intensity quickly, going to values under zero. After being darkened for some time, the nozzle's pixels start to increase their intensity due to the formation of the liquid stream in the injector axis and its illumination by the MIE light beams. For mild collapse conditions, the time to reach the maximum intensity is longer before it drops to zero and negative values. This happens due to the fuel taking longer to cloud the nozzle sight. In those cases, when the pixel intensities average is 0 again, the spray is considered to be collapsed. These intensity curves over time help to gain a different insight into the collapse mechanism's transients that appear on GDI injectors.

If all the collapse instants are recorded, as explained before, using the nozzle pixel intensity monitoring, a new figure can be created condensing all the test conditions. Fig. 18 shows the collapse times against R_p for all fuels and test conditions. Note that it shows only $R_p > 1$ since the collapse is only approached here through flash boiling cases. Inside the figure, the SOI and EOI times are marked, which are important when explaining the different collapse behaviors. From the Figure, three different zones are seen depending on the collapse time. Du et al. [10] also reported three collapse regions based on the average optical thickness of DBI images.

In Fig. 18 the first zone is situated close to the SOI line. Here, the most extreme collapsing cases are encountered, which indicate that the spray plumes collapsed from the very injection start. This zone is dominated by the lowest discharge pressure tested, and the resulting flashing conditions led to wider sprays, provoking high interaction between the spray plumes, and resulting in an almost instantaneous collapse. At these conditions, a high fuel concentration in the boundaries between two spray plumes can be observed as depicted in Fig. 13. The next

zone is located between the SOI and EOI. There is collapse for these conditions; however, the interaction between plumes is insufficient for a strong collapse, so as the spray develops, the jets get wider and the full interaction and collapse happen further downstream. The last location is referred to the conditions in which "collapse" occurs close to the EOI line. The "collapse" in this last zone does not appear on a stationary spray. Nevertheless, as the injector needle closes, the last liquid fuel coming out of the orifices is attracted to the nozzle axis, probably because there is a slightly low-pressure zone in that area due to the weak interaction between plumes, which, although not sufficient to collapse the sprays, allows that some fuel concentration appears at the nozzle axis, giving the impression of being a collapse from the nozzle pixel intensity diagnostic point of view.

4. Conclusions

Two different optical techniques were employed to analyze the spray collapse due to flash boiling on the ECN Spray G injector. Four surrogate mono-component fuels were tested with different molecular weights and volatile properties in order to investigate more extreme flashing conditions. Through the approaches employed, the instant at which the spray collapsed and the degree of collapse were quantified.

The findings can be summarized as follows:

- From the spray width curves, two collapse structures could appear at flashing conditions: the transitional collapse and severe collapse. The transitional collapse showed a greater spray expansion in the first millimeters from the nozzle.
- For the fuels employed, the most volatile ones yielded an early collapse for the same test condition.
- The instantaneous spray width variation for a stabilized jet was strongly correlated to the degree of collapse. Thresholds for classifying transitional and strong collapse injection conditions were determined.
- The nucleation theory and phase change potential were used to relate the spray expansion at different flashing and non-flashing conditions. The spray width at different distances from the nozzle exit was observed to have good agreement with R_p smaller than 3.5.
- A clear relation between the parameter X from the nucleation theory and the spray width was not found. The relations were reasonable for close distances to the nozzle until 20d - 40d; however, further distances did not appropriately correlate. The nucleation rate appeared to be a less influential expansion mechanism for internal flashing sprays. It was probably dominated by other mechanisms, such as aerodynamic forces and droplets diffusion into the air.
- The instant at which the spray collapsed was quantified by monitoring the clouding of the nozzle tip by the fuel, using the MIE frontal visualization.
- The spray surface evolution demonstrated a strong correlation with the R_p at each T_f when the spray was stabilized. Nonetheless, this correlation was no longer valid at high R_p when the spray collapsed, which happened at a similar R_p independently of the fuel tested.
- Three main collapse instants were observed:

    1. First, the typical collapse structure, in which the sprays collide into the center almost at the same instant that the injection starts.
    2. Secondly, for mild collapse conditions. The collapse occurred after the spray had developed to some extent.
    3. Finally, for flashing conditions, the nozzle was also clouded at the end of the injection. This result proposed that the inner low-pressure zone induced by plume-to-plume interaction was present. Although not sufficient to collapse, the last flow exiting the nozzle is suctioned to the spray axis.

Declaration of competing interest

The authors declare that they have no known competing financial interests or personal relationships that could have appeared to influence the work reported in this paper.

Data availability

Data will be made available on request.

Acknowledgments

This work was funded by the Spanish Ministerio de Ciencias e Innovación through project reference PID2021-1258120B-C21. The author Victor Mendoza thanks the Universitat Politècnica de València for his predoctoral contract, which is included within the framework of "Programa Propio de la Universitat Politècnica de València - Subprograma 1 (PAID-01-20)".

References

[1] A. Kalwar, A.K. Agarwal, Optical Diagnostics for Gasoline Direct Injection Engines, Springer Singapore, Singapore, 2022, pp. 201–241, http://dx.doi.org/10.1007/978-981-16-8418-0_7.

[2] Z. Li, S. Mi, Y. Zhang, Y. Qian, X. Lu, Characterizing the role of fuel injection strategies on performance, combustion, and emissions in intelligent charge compression ignition (icci) mode, Appl. Therm. Eng. 207 (2022) 118169, http://dx.doi.org/10.1016/j.applthermaleng.2022.118169.

[3] E. Shafiei, R. Dauphin, M. Yugo, Optimal electrification level of passenger cars in europe in a battery-constrained future, Transp. Res. D 102 (2022) 103132, http://dx.doi.org/10.1016/j.trd.2021.103132, URL: https://www.sciencedirect.com/science/article/pii/S1361920921004272.

[4] A. Hassani, A. Maleki, Projection of passenger cars' fuel demand and greenhouse gas emissions in iran by 2050, Energy Convers. Manag.: X 12 (2021) 100126, http://dx.doi.org/10.1016/j.ecmx.2021.100126.

[5] M. Krämer, E. Kull, M. Wensing, Flash boiling-induced targeting changes in gasoline direct injection sprays, Int. J. Engine Res. 17 (2016) 97–107, http://dx.doi.org/10.1177/1468087415604763.

[6] M. Chang, Z. Lee, S. Park, S. Park, Characteristics of flash boiling and its effects on spray behavior in gasoline direct injection injectors: A review, Fuel 271 (2020) 117600, http://dx.doi.org/10.1016/j.fuel.2020.117600.

[7] R. Kale, R. Banerjee, Experimental investigation on gdi spray behavior of isooctane and alcohols at elevated pressure and temperature conditions, Fuel 236 (2019) 1–12, http://dx.doi.org/10.1016/j.fuel.2018.08.153.

[8] E. Sher, T. Bar-Kohany, A. Rashkovan, Flash-boiling atomization, Prog. Energy Combust. Sci. 34 (2008) 417–439, http://dx.doi.org/10.1016/j.pecs.2007.05.001.

[9] H. Guo, Y. Li, B. Wang, H. Zhang, H. Xu, Numerical investigation on flashing jet behaviors of single-hole GDI injector, Int. J. Heat Mass Transfer 130 (2019) 50–59, http://dx.doi.org/10.1016/j.ijheatmasstransfer.2018.10.088.

[10] J. Du, B. Mohan, J. Sim, T. Fang, W.L. Roberts, Study of spray collapse phenomenon at flash boiling conditions using simultaneous front and side view imaging, Int. J. Heat Mass Transfer 147 (2020) 118824, http://dx.doi.org/10.1016/j.ijheatmasstransfer.2019.118824.

[11] F. Duronio, A. De Vita, A. Montanaro, C. Villante, Gasoline direct injection engines – A review of latest technologies and trends. Part 2, Fuel 265 (2020) 116947, http://dx.doi.org/10.1016/j.fuel.2019.116947.

[12] A. Rurik, F. Otto, T. Koch, Strategy and potential of homogeneous lean combustion at high load points for turbocharged gasoline engines with direct injection and small displacement, Automot. Engine Technol. 5 (2020) http://dx.doi.org/10.1007/s41104-020-00061-2.

[13] A. Kalwar, A.K. Agarwal, Lean-Burn Combustion in Direct-Injection Spark-Ignition Engines, Springer Singapore, Singapore, 2021, pp. 281–317, http://dx.doi.org/10.1007/978-981-16-1513-9_12.

[14] Z. Sun, M. Cui, C. Ye, S. Yang, X. Li, D. Hung, M. Xu, Split injection flash boiling spray for high efficiency and low emissions in a gdi engine under lean combustion condition, Proc. Combust. Inst. 38 (2021) 5769–5779, http://dx.doi.org/10.1016/j.proci.2020.05.037.

[15] Z. Sun, H. Wang, M. Cui, M. Nour, X. Li, M. Xu, Investigation of flash boiling injection schemes in lean-burn gasoline direct injection engines, Appl. Energy Combust. Sci. 7 (2021) 100035, http://dx.doi.org/10.1016/j.jaecs.2021.100035.

[16] C. Jiang, M.C. Parker, J. Helie, A. Spencer, C.P. Garner, G. Wigley, Impact of gasoline direct injection fuel injector hole geometry on spray characteristics under flash boiling and ambient conditions, Fuel 241 (2019) 71–82, http://dx.doi.org/10.1016/j.fuel.2018.11.143.

[17] M. Chang, Y.S. Yu, S. Park, S. Park, Spray dynamics and atomization characteristics of multi-hole gdi injectors under flash boiling conditions, Appl. Therm. Eng. 200 (2022) 117626, http://dx.doi.org/10.1016/j.applthermaleng.2021.117626.

[18] P.G. Aleiferis, Z.R. Van Romunde, An analysis of spray development with iso-octane, n-pentane, gasoline, ethanol and n-butanol from a multi-hole injector under hot fuel conditions, Fuel 105 (2013) 143–168, http://dx.doi.org/10.1016/j.fuel.2012.07.044.

[19] F. Duronio, A. De Vita, L. Allocca, M. Anatone, Gasoline direct injection engines – A review of latest technologies and trends. Part 1: Spray breakup process, Fuel 265 (2020) 116948, http://dx.doi.org/10.1016/j.fuel.2019.116948.

[20] M. Nour, Z. Sun, M. Cui, S. Yang, D. Hung, X. Li, M. Xu, Effect of flash boiling injection on combustion and PN emissions of DISI optical engine fueled with butanol isomers/TPRF blends, Proc. Combust. Inst. 38 (2021) 5923–5931, http://dx.doi.org/10.1016/j.proci.2020.10.006.

[21] Y. Li, H. Guo, S. Fei, X. Ma, Z. Zhang, L. Chen, L. Feng, Z. Wang, An exploration on collapse mechanism of multi-jet flash-boiling sprays, Appl. Therm. Eng. 134 (2018) 20–28, http://dx.doi.org/10.1016/j.applthermaleng.2018.01.102.

[22] A. Bautista Rodríguez, Study of the Gasoline Direct Injection Process under Novel Operating Conditions (Ph.D. thesis), Universitat Politècnica de València, 2021.

[23] J. Yan, S. Gao, W. Zhao, T.H. Lee, C.-F. Lee, Experimental study of sprays with isooctane, hexane, ethanol and their binary mixtures under different flash boiling intensities, Int. J. Heat Mass Transfer 179 (2021) 121715, http://dx.doi.org/10.1016/j.ijheatmasstransfer.2021.121715.

[24] W. Zhao, J. Yan, S. Gao, T.H. Lee, X. Li, Effects of fuel properties and aerodynamic breakup on spray under flash boiling conditions, Appl. Therm. Eng. 200 (2022) 117646, http://dx.doi.org/10.1016/j.applthermaleng.2021.117646.

[25] R. Kale, R. Banerjee, Spray Collapse in a Multi-Hole GDI Injector and Its Effect on in-Cylinder Combustion, Springer Singapore, Singapore, 2019, pp. 43–61, http://dx.doi.org/10.1007/978-981-13-3256-2_3.

[26] W. Liu, Y. Lu, Y. Kang, J. Yan, C.-F. Lee, Macroscopic characteristics of flash-boiling spray focused on plume interaction, Int. J. Heat Mass Transfer 170 (2021) 120999, http://dx.doi.org/10.1016/j.ijheatmasstransfer.2021.120999, URL: https://www.sciencedirect.com/science/article/pii/S0017931021001022.

[27] G. Di Ilio, V.K. Krastev, G. Falcucci, Evaluation of a scale-resolving methodology for the multidimensional simulation of gdi sprays, Energies 12 (2019).

[28] Engine combustion network, 2010, https://ecn.sandia.gov/diesel-spray-combustion/ Online.

[29] Y. Huang, G. Hong, R. Huang, Numerical investigation to the dual-fuel spray combustion process in an ethanol direct injection plus gasoline port injection (EDI + GPI) engine, Energy Convers. Manage. 92 (2015) 275–286, http://dx.doi.org/10.1016/j.enconman.2014.12.064.

[30] K. Kar, T. Last, C. Haywood, R. Raine, Measurement of vapor pressures and enthalpies of vaporization of gasoline and ethanol blends and their effects on mixture preparation in an SI engine, SAE Int. J. Fuels Lubr. 1 (2009) 132–144, http://dx.doi.org/10.4271/2008-01-0317.

[31] E.W. Lemmon, M.O. McLinden, D.G. Friend, Thermophysical properties of fluid systems, in: P.J. Linstrom, W.G. Mallard (Eds.), NIST Chemistry WebBook, NIST Standard Reference Database Number 69, 2011.

[32] J. Du, H. Chen, Y. Li, L. Ye, G. Li, Experimental study on ethanol gasoline flash-boiling spray characteristics using multi-hole gdi injector, in: Proceedings of China SAE Congress 2019: Selected Papers, Springer Singapore, Singapore, 2021, pp. 635–645.

[33] D. Vaquerizo, Study on Advanced Spray-Guided Gasoline Direct Injection Systems (Ph.D. thesis), Universitat Politècnica de València, 2017.

[34] J.B. Ghandhi, D.M. Heim, An optimized optical system for backlit imaging, Rev. Sci. Instrum. 80 (2009) 056105, http://dx.doi.org/10.1063/1.3128728.

[35] D.F. Swinehart, The beer-lambert law, J. Chem. Educ. 39 (1962) 333.

[36] C. Geschwindner, P. Kranz, C. Welch, M. Schmidt, B. Böhm, S.A. Kaiser, J. De la Morena, Analysis of the interaction of spray g and in-cylinder flow in two optical engines for late gasoline direct injection, Int. J. Engine Res. 21 (2020) 169–184, http://dx.doi.org/10.1177/1468087419881535.

[37] R. Payri, J.M. García-Oliver, V. Mendoza, A. Viera, Analysis of the influence of diesel spray injection on the ignition and soot formation in multiple injection strategy, Energies 13 (2020) http://dx.doi.org/10.3390/en13133505.

[38] R. Payri, G. Bracho, P. Marti-Aldaravi, A. Viera, Near field visualization of diesel spray for different nozzle inclination angles in non-vaporizing conditions, At. Sprays 27 (2017) 251–267, http://dx.doi.org/10.1615/AtomizSpr.2017017949.

[39] R. Payri, F.J. Salvador, G. Bracho, A. Viera, Differences between single and double-pass schlieren imaging on diesel vapor spray characteristics, Appl. Therm. Eng. 125 (2017) 220–231, http://dx.doi.org/10.1016/j.applthermaleng.2017.06.140.

[40] A. Viera, Effect of Multiple Injection Strategies on the Diesel Spray Formation and Combustion using Optical Diagnostics (Ph.D. thesis), Universitat Politècnica de València, 2019.

[41] R. Payri, F.J. Salvador, P. Martí-Aldaraví, D. Vaquerizo, ECN Spray G external spray visualization and spray collapse description through penetration and morphology analysis, Appl. Therm. Eng. 112 (2017) 304–316, http://dx.doi.org/10.1016/j.applthermaleng.2016.10.023.

[42] H. Guo, B. Wang, Y. Li, H. Xu, Z. Wu, Characterizing external flashing jet from single-hole GDI injector, Int. J. Heat Mass Transfer 121 (2018) 924–932, http://dx.doi.org/10.1016/j.ijheatmasstransfer.2018.01.042.

[43] Y. Li, H. Guo, Z. Zhou, Z. Zhang, X. Ma, L. Chen, Spray morphology transformation of propane, n-hexane and iso-octane under flash-boiling conditions, Fuel 236 (2019) 677–685, http://dx.doi.org/10.1016/j.fuel.2018.08.160.

[44] X. Li, Q. Xu, S. Qiu, S. Wang, D. Hung, M. Xu, Investigations on the impact of phase change on single plume flash boiling radial expansion and drop-sizing characteristics, Appl. Therm. Eng. 202 (2022) 117911, http://dx.doi.org/10.1016/j.applthermaleng.2021.117911.

[45] H. Guo, Y. Li, X. Lu, Z. Zhou, H. Xu, Z. Wang, Radial expansion of flash boiling jet and its relationship with spray collapse in gasoline direct injection engine, Appl. Therm. Eng. 146 (2019) 515–525, http://dx.doi.org/10.1016/j.applthermaleng.2018.10.031.

[46] C. Devos, T. Van Gerven, S. Kuhn, A review of experimental methods for nucleation rate determination in large-volume batch and microfluidic crystallization, Cryst. Growth Des. 21 (2021) 2541–2565, http://dx.doi.org/10.1021/acs.cgd.0c01606.

[47] R.D. Oza, J.F. Sinnamon, An Experimental and Analytical Study of Flash-Boiling Fuel Injection, SAE Technical Papers 1983, http://dx.doi.org/10.4271/830590.

[48] S.L. Girshick, C.P. Chiu, Kinetic nucleation theory: A new expression for the rate of homogeneous nucleation from an ideal supersaturated vapor, J. Chem. Phys. 93 (1990) 1273–1277, http://dx.doi.org/10.1063/1.459191.

[49] G. Job, F. Herrmann, Chemical potential - A quantity in search of recognition, Eur. J. Phys. 27 (2006) 353–371, http://dx.doi.org/10.1088/0143-0807/27/2/018.

[50] H. Guo, H. Ding, Y. Li, X. Ma, Z. Wang, H. Xu, J. Wang, Comparison of spray collapses at elevated ambient pressure and flash boiling conditions using multi-hole gasoline direct injector, Fuel 199 (2017) 125–134, http://dx.doi.org/10.1016/j.fuel.2017.02.071.

[51] M. Martínez García, Computational Study of the Injection Process in Gasoline Direct Injection (GDI) Engines (Ph.D. thesis), Universitat Politècnica de València, 2022.

[52] J.D. Naber, D.L. Siebers, Effects of Gas Density and Vaporization on Penetration and Dispersion of Diesel Sprays, Vol. 105, SAE Paper 960034, Society of Automotive Engineers, Inc., Warrendale, Pennsylvania, USA, 1996, pp. 82—-111, http://dx.doi.org/10.4271/960034.

[53] H. Guo, Y. Li, X. Lu, Z. Zhou, H. Xu, Z. Wang, Radial expansion of flash boiling jet and its relationship with spray collapse in gasoline direct injection engine, Appl. Therm. Eng. 146 (2019) 515–525, http://dx.doi.org/10.1016/j.applthermaleng.2018.10.031.

[54] B.S. Park, S.Y. Lee, An experimental investigation of the flash atomization mechanism, At. Sprays (1994) http://dx.doi.org/10.1615/atomizspr.v4.i2.30.

[55] R. Payri, G. Hardy, J. Gimeno, A. Bautista, Analysis of counterbore effect in five diesel common rail injectors, Exp. Therm Fluid Sci. 107 (2019) 69–78, http://dx.doi.org/10.1016/j.expthermflusci.2019.05.008.

[56] S. Wu, A. Gandhi, H. Li, M. Meinhart, Experimental and numerical study of the effects of nozzle taper angle on spray characteristics of gdi multi-hole injectors at cold condition, Fuel 275 (2020) 117888, http://dx.doi.org/10.1016/j.fuel.2020.117888.

[57] H. Oh, J. Hwang, L. White, L.M. Pickett, D. Han, Spray collapse characteristics of practical gdi spray for lateral-mounted gdi engines, Int. J. Heat Mass Transfer 190 (2022) 122743, http://dx.doi.org/10.1016/j.ijheatmasstransfer.2022.122743.

[58] M.R. Vetrano, A. Simonini, J. Steelant, P. Rambaud, Thermal characterization of a flashing jet by planar laser-induced fluorescence this article is part of the topical collection on application of laser techniques to fluid mechanics 2012, Exp. Fluids 54 (2013) http://dx.doi.org/10.1007/s00348-013-1573-8.

[59] P. Sphicas, L.M. Pickett, S.A. Skeen, J.H. Frank, Inter-plume aerodynamics for gasoline spray collapse, Int. J. Engine Res. (2018) http://dx.doi.org/10.1177/1468087417740306.

[60] Y. Li, H. Guo, X. Ma, Y. Qi, Z. Wang, H. Xu, S. Shuai, Morphology analysis on multi-jet flash-boiling sprays under wide ambient pressures, Fuel 211 (2018) 38–47, http://dx.doi.org/10.1016/j.fuel.2017.08.082.